ChemComm

Low Temperature and Limited Water Activity Reveal a Pathway to Magnesite via Amorphous Magnesium Carbonate

Journal:	*ChemComm*
Manuscript ID	CC-COM-07-2020-004907.R1
Article Type:	Communication

COMMUNICATION

Low Temperature and Limited Water Activity Reveal a Pathway to Magnesite via Amorphous Magnesium Carbonate†

Received 00th January 20xx,
Accepted 00th January 20xx

DOI: 10.1039/x0xx00000x

Sebastian T. Mergelsberg [a], Sebastien N. Kerisit [a], Eugene S. Ilton [a], Odeta Qafoku [b], Christopher J. Thompson [c], and John S. Loring*[a]

Forsterite carbonated in thin H_2O films to magnesite via amorphous magnesium carbonate during reaction with H_2O-bearing liquid CO_2 at 25 °C. This novel reaction pathway contrasts with previous studies that were carried out at higher H_2O activity and temperature, where more highly hydrated nesquehonite was the metastable intermediate.

Chemistry in low water environments that can prevail, for example, in the Earth's atmosphere and vadose zones, is facilitated by molecularly thin H_2O films on hydrophilic mineral surfaces.[1-4] At equilibrium, the activity of H_2O in these films is dictated by the chemical potential of H_2O in the gas phase (or some bulk fluid phase) and can range from near zero to that of pure bulk water. Further, H_2O-mineral and H_2O-gas/fluid interfaces affect the properties of H_2O by disrupting hydrogen bonding and limiting rotational/translational degrees of freedom, with implications for complexation, diffusion, and mineral reactivity in thin H_2O films.[5, 6] Indeed, prior work has correlated threshold H_2O film thicknesses to the onset of diffusion, dissolution of the primary phase, and precipitation of alteration products.[7, 8] In contrast, given high mineral-surface-to-water-volume ratios, relatively minor amounts of mineral dissolution can rapidly yield high ionic strength and high degrees of oversaturation with respect to secondary phases.[9] In sum, the properties of thin H_2O films lead to mineral transformation pathways that deviate from those in bulk water.

A recent example of unique reactivity in H_2O films is the low temperature formation of magnesite ($MgCO_3$) and SiO_2 during the carbonation of forsterite (Mg_2SiO_4) in humidified supercritical CO_2 ($scCO_2$). Divalent metal silicate carbonation is a process important for permanent CO_2 storage in geologic reservoirs.[4, 10, 11] Although magnesite is the most thermodynamically stable magnesium carbonate, it is rarely observed at temperatures below 60 °C in aqueous solution, likely due to the slow H_2O exchange rate and large hydration energy of the Mg^{2+} cation.[12, 13] Yet, Felmy et al.[14] and Qafoku et al.[15] showed that forsterite carbonated to magnesite at 35 °C in thin H_2O films in $scCO_2$ at 100% relative humidity (RH) through the metastable intermediate, nesquehonite ($MgCO_3{\cdot}3H_2O$). Similarly, Miller et al.[8] recently reported carbonation of forsterite to magnesite via nesquehonite at 50 °C and 100% RH in $scCO_2$. Interestingly, similar experiments at 85% RH produced magnesite, but nesquehonite was not detected, possibly because the lower H_2O activity was not conducive to nesquehonite stability.[8]

The goal of this study was to further investigate the low temperature and low H_2O activity carbonation pathway of forsterite in thin H_2O films. Experiments were carried out at 25 °C in H_2O-bearing liquid CO_2 using a combination of in-situ infrared (IR) spectroscopy and ex-situ scanning electron microscopy (SEM), high-energy X-ray diffraction (heXRD), and pair distribution function (PDF) characterization. We used nearly the lowest H_2O activity in the CO_2 phase that would still yield a H_2O film thickness on forsterite just greater than the threshold of 1.5 monolayer (ML) needed for dissolution and carbonate precipitation (see below).[7] Pushing the limits of this process to 25 °C and low H_2O activity is part of a larger research effort to understand what properties of thin H_2O films are conducive to low-temperature magnesite formation. Here, we show for the first time that magnesite grows in thin H_2O films at 25 °C, after the formation of an amorphous magnesium carbonate (AMC; $MgCO_3 \cdot xH_2O$, $0.5 < x < 1$) precursor.[16]

We used in-situ IR spectroscopic titrations to monitor the carbonation of forsterite. In this technique, known volumes of water are added stepwise to a CO_2-pressurized vessel equipped with both transmission and attenuated total reflection (ATR) IR optics. Titration specifics are summarized in Table S1. Titration 25C_Cal (Figure S1) was the control experiment of a CO_2-pressurized vessel in the absence of forsterite. Transmission IR was used to correlate the absorbance of the HOH bend of H_2O to H_2O concentration in the fluid; the concentration of H_2O at saturation was 56 ± 1 mM, in reasonable agreement with a value of 57.4 mM predicted by the model of Spycher et al.[17] Titration 25C_Titra (Figure S1) was of 0.22067 g forsterite and used transmission IR to correlate H_2O coverage to fluid percent H_2O saturation (Figure S1b). Titration 25C_Time_Dep was of ~0.005 g of forsterite adhered as an overlayer on the ATR IR internal reflection element. Water was added until the H_2O

[a] Physical and Computational Sciences Directorate, Pacific Northwest National Laboratory, Richland, WA 99354, United States E-mail: john.loring@pnnl.gov
[b] Earth and Biological Sciences Directorate, Pacific Northwest National Laboratory, Richland, WA 99354, United States
[c] Energy and Environment Directorate, Pacific Northwest National Laboratory, Richland, WA 99354, United States

†Electronic Supplementary Information (ESI) available: Experimental methods, Tables S1 and S2 and Figures S1–S6; See DOI: 10.1039/x0xx00000x

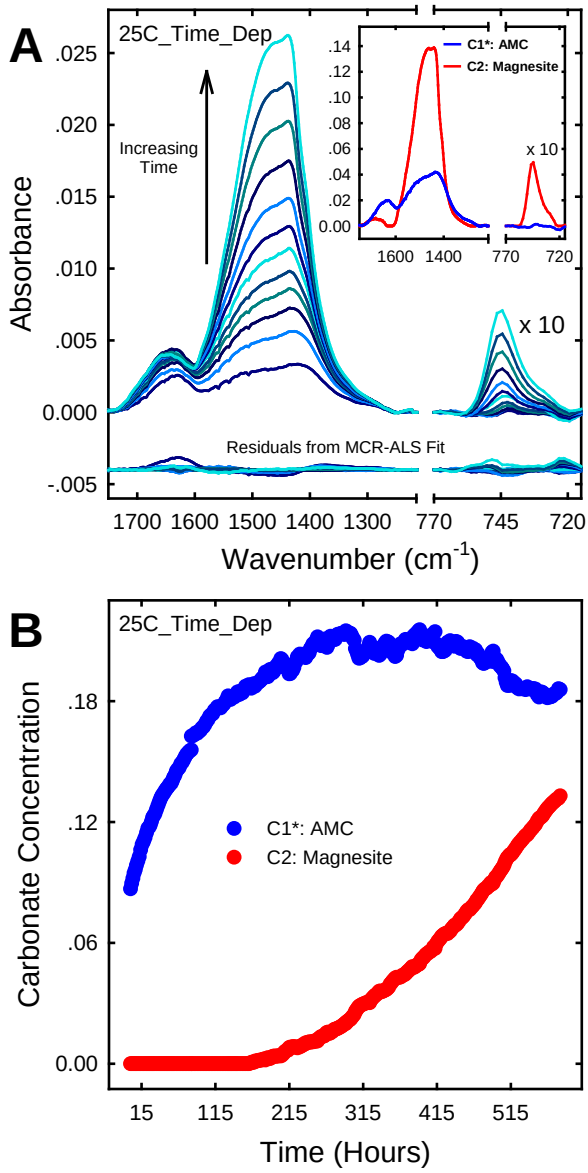

Figure 1. (A) Examples of ATR IR spectra at 53 hour increments from 0 to 582 hours in the CO deformation (715 to 770 cm^{-1}) and asymmetric CO stretching (1215 to 1600 cm^{-1}) regions of carbonate as a function of time after reaching fluid H_2O saturation of 64% (a H_2O coverage on the forsterite of 1.8 ML) during experiment 25C_Time_Dep (see Table S1), in which forsterite was titrated with H_2O in liquid CO_2 at 25 °C and 90 bar. Spectra were fit using a two-component MCR-ALS analysis. The inset shows components C1 and C2, which are assigned to AMC and magnesite, respectively (see also Figure S2). The MCR-ALS derived relative concentrations of components C1 and C2 as a function time are in (B). The * next to C1 indicates that its spectrum and concentration have been scaled using a measured absorption coefficient ratio as described in the main text (see also Figures S3 and S4).

coverage was above a measured threshold of 1.5 ML needed for carbonate precipitation.[7] While (bi)carbonate surface complexes predominate below 1.5 ML, carbonates precipitate above this threshold coverage because the H_2O film is thick enough to enable the transport of ions (e.g., Mg^{2+} and HCO_3^-) to nucleation sites for carbonate growth.[7, 18] Accordingly, we stopped H_2O additions at 64% H_2O saturation, corresponding to a H_2O coverage of 1.8 ML (Figure S2b) and collected for the next 24 days. Examples of ATR IR spectra are shown in Figure 1a. The background spectrum for these data is of forsterite at 0% H_2O saturation, which effectively removes most of the spectral contributions from (bi)carbonate surface complexes. Notable changes with increasing time included a narrowing of the asymmetric CO stretching bands between 1275 and 1600 cm^{-1}.

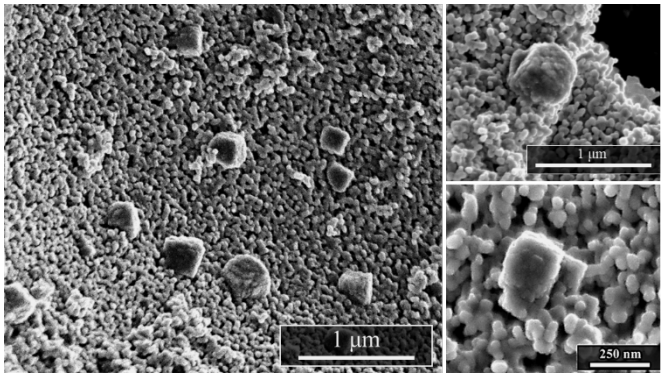

Figure 2. SEM images of the postreacted sample from experiment 25C_Time_Dep where forsterite was carbonated in CO_2 at 25 °C and 90 bar at 64% H_2O saturation (H_2O coverage of 1.82 ML) for 24 days. Precipitated magnesite crystals with irregular facets have a particle size of 250-450 nm.

A multivariate curve resolution alternating least squares (MCR-ALS) analysis of the ATR IR spectra from 25C_Time_Dep in the asymmetric CO stretching and CO deformation regions modelled 99.95% of the variance as a linear combination of the two components shown in the inset of Figure 1a. Component C1 contained no CO deformation band at 746 cm^{-1} and is assigned to amorphous magnesium carbonate (AMC) by comparison to the spectrum of synthetic AMC (Figure S2; see Methods in Supporting Information). Component C2 is assigned to magnesite by comparison to a standard spectrum of magnesite (Figure S2) formed from a forsterite sample fully carbonated at 50 °C and 90 bar $scCO_2$ in bulk water (experiment 50C_Fully_React; see Table S1). This component spectrum had the CO deformation band at 746 cm^{-1}, which is diagnostic for magnesite[19], and it also had minimal absorbance of the HOH bend of H_2O between 1600 and 1770 cm^{-1}, consistent with no structural H_2O in magnesite. The concentrations of these components as a function of time are shown in Figure 1b. It should be noted that the spectrum and concentrations of AMC (C1) have been scaled relative to magnesite (C2) using an absorption coefficient ratio that was determined using the results of a second MCR-ALS analysis in the SiO stretching regions of forsterite and precipitated amorphous SiO_2 (see Figures S3 and S4 for details). The mole ratio of AMC to magnesite at the end of experiment 25C_Time_Dep is 1.4 to 1.

SEM images of the postreacted forsterite from 25C_Time_Dep are shown in Figure 2 and provide further confirmation that magnesite nucleated and grew. The forsterite is an aggregate of 10-30 nm sized particulates. Upright from the forsterite surface, magnesite crystals are observed that have irregular facets and are 250-450 nm in size. The magnesite is randomly scattered on the forsterite aggregates, which suggests there is no preferential nucleation and growth of $MgCO_3$ in relation to the topography of the forsterite surface. There is no evidence of a separate AMC phase. This could be because the AMC has a similar particle size and morphology as

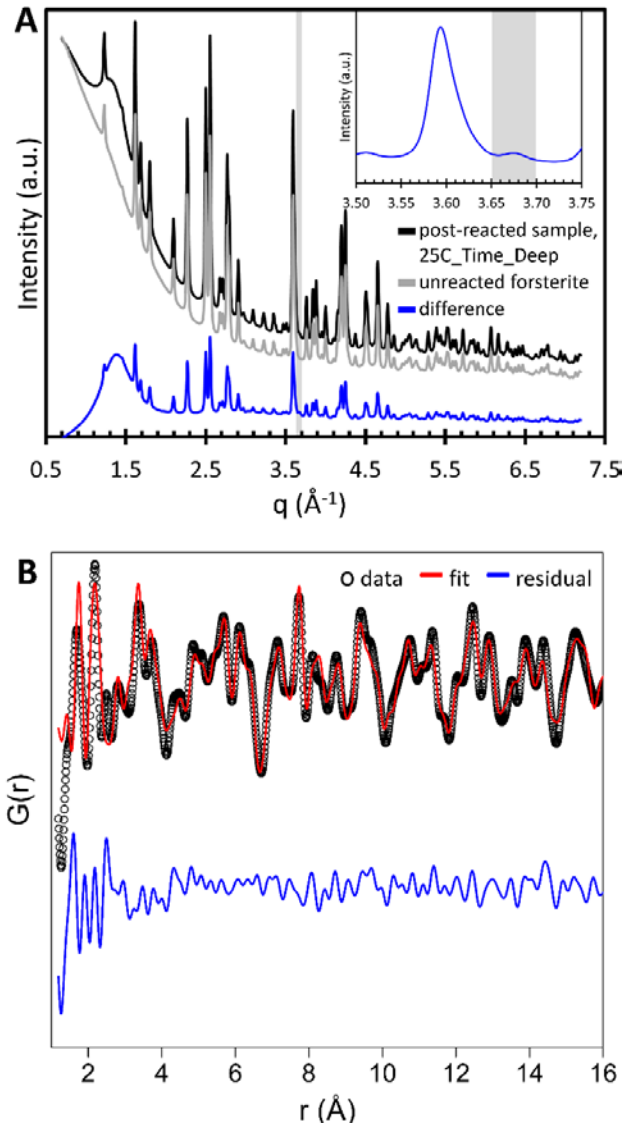

Figure 3. (A) High-energy X-ray diffraction of unreacted forsterite (grey), the postreacted sample from titration 25C_Time_Dep (black), and the difference pattern (blue). The inset highlights the highest intensity magnesite peak, which confirms the precipitation of this carbonate. (B) Linear combination fit (red) of PDF data of the postreacted sample (black circles) and the residual (blue). All intermediate fits are shown in Figs. S5, S6, and S7, and analysis results are summarized in Table S2.

the forsterite or because it precipitates as a coating on the individual forsterite particles.

The heXRD of the postreacted forsterite from 25C_Time_Dep also confirms magnesite precipitation (Fig. 3A, grey vertical line, inset). Furthermore, subtraction of unreacted forsterite from the sample pattern indicated a considerable amount of amorphous material. Some remaining forsterite in the difference pattern is most likely due to variability in packing density during sample preparation. To quantify the composition of the sample, the heXRD peaks were fit and compared to a refinement of forsterite and magnesite to the PDF data (See SI for detailed procedure). Refinement of the heXRD pattern of 25C_Time_Dep determines that approximately 1.7 mol% magnesite formed (Fig. 3A, Table S2). A similar fit to the PDF pattern (Figure S7b) yields 0.88 mol% magnesite, but an analysis of the residual reveals a substantial contribution of forsterite signal and a significantly underestimated Mg-O atom pair at 2.2 Å, indicating the presence of AMC (Fig S8). To determine the total composition including the amorphous phases, the PDF of 25C_Time_Dep in Figure 3b was fit using a linear combination approach with the refined forsterite and magnesite structures from the Rietveld refinement, as well as the experimental PDF of synthetic AMC and the magnesite-subtracted PDF pattern of fully reacted forsterite from 50C_Fully_React. Results indicate the amorphous component makes up approximately 20 mol% of the sample, which is consistent with the large amorphous feature observed in Figure 3a. The mole ratio of AMC to magnesite is either 6 or 10, depending on the assumed hydration states of the AMC and amorphous SiO_2 (see SI), which is considerably larger than measured by IR spectroscopy.

The discrepancy in composition between IR and X-ray analyses is likely due to technique-specific sensitivities to amorphous phases. Carbonation of forsterite in the presence of a thin H_2O film likely causes the formation of a large number of short-range order dominant phases. These include adsorbed species, solvated ions, disordered mineral interfaces, and surface complexes, which all contribute to the short-range order measured by PDF analysis (Figure 3B). For example, the Si-O bond distance (~1.6 Å) is overestimated in both length and abundance in Figure 3B, while the amplitude of the Mg-O distance (~2.1 Å) is underestimated. Further, a peak at 2.7 is completely missed by the four components used in the fitting procedure. This indicates there are multiple short-range ordered phases present besides silica and AMC that cause a relative underestimation of the molar abundance of total amorphous phases. On the other hand, IR is likely insensitive to these intermediate structures and may thus be biased towards crystalline phases and near-bulk amorphous phases.

To our knowledge, this is the first time the AMC to magnesite transformation has been reported.[20, 21] Further, nesquehonite was not detected in experiment 25C_Time_Dep, in contrast with similar experiments in previous studies but at higher H_2O activity and temperature.[8, 14, 15, 22] We hypothesize that the selective precipitation of AMC versus nesquehonite was due to the comparatively lower H_2O activity in thin H_2O films achieved by carbonating at 64% H_2O saturation. While the solubilities of nesquehonite and AMC in aqueous solution are similar at 25 °C ($\log_{10}K_{sp}$ = -5.25 for nesquehonite[23]; -4.54[16] to -5.48[24] for AMC), the ion activity product of nesquehonite depends on the cube of the H_2O activity, versus only a power of 0.5 to 1 for AMC. Hence, lower H_2O activity favors AMC over nesquehonite at otherwise the same Mg^{2+} and CO_3^{2-} reactant concentrations. We suggest that nesquehonite was not observed in 25C_Time_Dep because either the H_2O film never became supersaturated with respect to nesquehonite, or it more quickly became supersaturated with respect to AMC so that AMC precipitated and grew much faster. Indeed, AMC grew as the sole metastable intermediate phase for more than 120 hours before magnesite nucleated (Figure 1b). Once magnesite started to grow, AMC formation competed with its transformation to magnesite. AMC persisted at a seemingly steady state concentration from about 230 to 420 hours, after which its rate of transformation to magnesite overtook its

growth rate. In sum, low temperature and limited H_2O activity fine-tuned the carbonation pathway of forsterite to magnesite through AMC, presumably bypassing the formation of nesquehonite. Future experiments will determine if nesquehonite indeed precipitates at higher H_2O activity during thin H_2O film carbonation of forsterite at 25 °C.

Magnesite growth is considered notoriously slow[13, 25], and thus its relatively fast growth in thin H_2O films is surprising. A recent study suggested that rapid magnesite growth in H_2O films is due to a unique mechanism involving Mg^{2+} coordinated by fewer than six inner-sphere waters.[26] Here, we suggest an alternative explanation that is in accordance with bulk studies. In aqueous solution, growth of micron-sized magnesite particles follows spiral growth kinetics, which are modeled by a rate constant multiplied by the square of the extent of supersaturation.[13, 25] Because AMC and magnesite coexist in experiment 25C_Time_Dep, we estimate that magnesite is supersaturated by at least two or perhaps three orders of magnitude, based on the solubility constants of magnesite[27] ($\log_{10}K_{sp}$ = -7.8, extrapolated to 25 °C) and AMC (see above). Hence, remarkably high reactant concentrations and a squared dependence on the extent of supersaturation could be the main drivers for why magnesite growth kinetics are seemingly enhanced in thin H_2O films. In fact, magnesite has been detected at 22 °C after 70 days in aqueous solutions supersaturated by a factor of only 28, albeit nucleated in the presence of carboxylated polystyrene microspheres.[28]

This study furthers an understanding of divalent silicate carbonation under low-H_2O CO_2-dominated fluids as part of a comprehensive effort to predict the fate of geologically stored CO_2. Future work will involve kinetic modeling of coupled forsterite dissolution and AMC/magnesite precipitation as a function of temperature to obtain activation energies for these processes that can be compared directly to bulk values.

This research was supported by the U.S. Department of Energy (DOE), Office of Science, Office of Basic Energy Sciences (BES), Chemical Sciences, Geosciences, and Biosciences Division through its Geosciences program at Pacific Northwest National Laboratory (PNNL). SEM analyses were performed at the Environmental Molecular Sciences Laboratory, a user facility sponsored by the DOE's Office of Biological and Environmental Research and located at PNNL. heXRD and PDF measurements were carried out at the Advanced Photon Source, a U.S. DOE Office of Science user facility operated by Argonne National Laboratory under Contract No. DE-AC02- 06CH11357. We thank Xin Zhang for synthesizing the AMC reference standard.

Conflicts of interest

There are no conflicts to declare.

Notes and references

1. M. J. Tang, D. J. Cziczo and V. H. Grassian, *Chem. Rev.*, 2016, **116**, 4205-4259.
2. M.-O. Goebel, J. Bachmann, M. Reichstein, B. Jansen and G. Guggenberger, *Global Change Biology*, 2011, **17**, 2640-2656.
3. S. K. Woche, M.-O. Goebel, R. Mikutta, C. Schurig, M. Kaestner, G. Guggenberger and J. Bachmann, *Sci Rep*, 2017, **7**, 42877.
4. J. S. Loring, Q. R. Miller, C. J. Thompson and H. T. Schaef, in *Science of Carbon Storage in Deep Saline Formations: Process Coupling Across Time and Spatial Scales*, eds. A. Ilgen and P. Newell, Elsevier, 2018, p. 336.
5. A. W. Knight, N. G. Kalugin, E. Coker and A. G. Ilgen, *Sci Rep*, 2019, **9**, 8246.
6. S. Le Caër, S. Pin, S. Esnouf, Q. Raffy, J. P. Renault, J. B. Brubach, G. Creff and P. Roy, *Phys. Chem. Chem. Phys.*, 2011, **13**, 17658-17666.
7. E. Placencia-Gómez, S. N. Kerisit, H. S. Mehta, O. Qafoku, C. J. Thompson, T. R. Graham, E. S. Ilton and J. S. Loring, *Environ. Sci. Technol.*, 2020, **54**, 6888-6899.
8. Q. R. S. Miller, J. P. Kaszuba, S. N. Kerisit, H. T. Schaef, M. E. Bowden, B. P. McGrail and K. M. Rosso, *Environ Sci Nano*, 2020, **7**, 1068-1081.
9. C. E. Wood, O. Qafoku, J. S. Loring and A. M. Chaka, *Environ. Sci. Technol. Lett.*, 2019, **6**, 592-599.
10. Y.-S. Jun, D. E. Giammar and C. J. Werth, *Environ. Sci. Technol.*, 2013, **47**, 3-8.
11. D. J. DePaolo, D. R. Cole, A. Navrotsky and I. C. Bourg, eds., *Geochemistry of Geologic Carbon Sequestration, Reviews in Mineralogy and Geochemistry Vol. 77*, 2013.
12. M. Hänchen, V. Prigiobbe, R. Baciocchi and M. Mazzotti, *Chem. Eng. Sci.*, 2008, **63**, 1012-1028.
13. G. D. Saldi, G. Jordan, J. Schott and E. H. Oelkers, *Geochim. Cosmochim. Acta*, 2009, **73**, 5646-5657.
14. A. R. Felmy, O. Qafoku, B. W. Arey, J. Z. Hu, M. Hu, H. Todd Schaef, E. S. Ilton, N. J. Hess, C. I. Pearce, J. Feng and K. M. Rosso, *Geochim. Cosmochim. Acta*, 2012, **91**, 271-282.
15. O. Qafoku, J. Hu, N. J. Hess, M. Y. Hu, E. S. Ilton, J. Feng, B. W. Arey and A. R. Felmy, *Geochim. Cosmochim. Acta*, 2014, **134**, 197-209.
16. B. Purgstaller, K. E. Goetschl, V. Mavromatis and M. Dietzel, *Crystengcomm*, 2019, **21**, 155-164.
17. N. Spycher, K. Pruess and J. Ennis-King, *Geochim. Cosmochim. Acta*, 2003, **67**, 3015-3031.
18. Q. R. S. Miller, D. A. Dixon, S. D. Burton, E. D. Walter, D. W. Hoyt, A. S. McNeill, J. D. Moon, K. S. Thanthiriwatte, E. S. Ilton, O. Qafoku, C. J. Thompson, H. T. Schaef, K. M. Rosso and J. S. Loring, *J. Phys. Chem. C*, 2019, **123**, 12871-12885.
19. H. A. Hans and F. K. Paul, *Am. Mineral.*, 1963, **48**, 124-137.
20. G. Montes-Hernandez and F. Renard, *Cryst. Growth Des.*, 2016, **16**, 7218-7230.
21. J. Tanaka, J. Kawano, T. Nagai and H. Teng, *J Miner Petrol Sci*, 2019, **114**, 105-109.
22. X. Zhang, A. S. Lea, A. M. Chaka, J. S. Loring, S. T. Mergelsberg, E. Nakouzi, O. Qafoku, J. J. De Yoreo, H. T. Schaef and K. M. Rosso, *Nature Materials*, 2020, Submitted.
23. A. L. Harrison, V. Mavromatis, E. H. Oelkers and P. Bénézeth, *Chem. Geol.*, 2019, **504**, 123-135.
24. S. T. Mergelsberg, J. J. DeYoreo, Q. R. S. Miller, F. M. Michel and P. M. Dove, *Geochim. Cosmochim. Acta*, 2020, DOI: 10.1016/j.gca.2020.1006.1030.
25. G. D. Saldi, J. Schott, O. S. Pokrovsky, Q. Gautier and E. H. Oelkers, *Geochim. Cosmochim. Acta*, 2012, **83**, 93-109.
26. Q. R. S. Miller, J. P. Kaszuba, H. T. Schaef, M. E. Bowden, B. P. McGrail and K. M. Rosso, *Chem. Commun.*, 2019, **55**, 6835-6837.
27. P. Bénézeth, G. D. Saldi, J.-L. Dandurand and J. Schott, *Chem. Geol.*, 2011, **286**, 21-31.
28. I. M. Power, P. A. Kenward, G. M. Dipple and M. Raudsepp, *Cryst. Growth Des.*, 2017, **17**, 5652-5659.

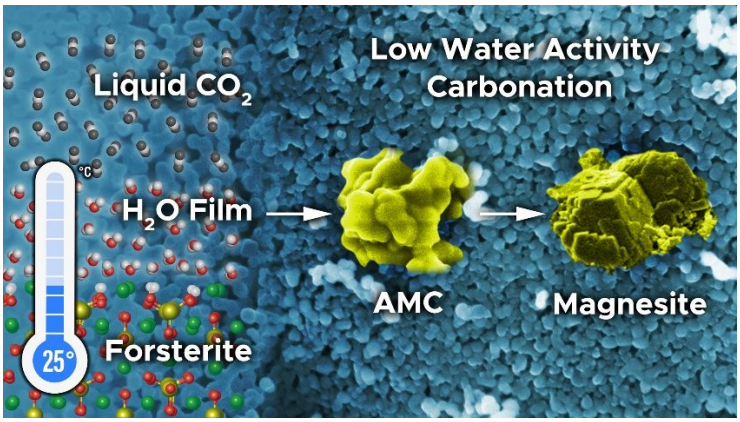

Experiments at low H_2O activity and 25 °C reveal a new reaction pathway to magnesite via amorphous magnesium carbonate during the thin H_2O film carbonation of forsterite in water-bearing liquid CO_2.